Nano Research

Open Access

Research Article

Hemoglobin integrated red blood cell membrane-coated metal-organic framework nano-platform for improving the self-adaptive blood glucose management

Shuai Wu[1], Li Zhu[1], Sheng Ni[1], Xiong Zhao[1], Meng Yan[1], Yuan Zhong[1], Karissa Kusuma[1], Yi Liang[1], Kaiwen Bao[1], Kai Qu[1,2], Xian Qin[1,2], Kun Zhang[1,2], Wuquan Deng[4] ✉, Da Sun[3] ✉, and Wei Wu[1] ✉

[1] *Key Laboratory of Biorheological Science and Technology, Ministry of Education, College of Bioengineering, Chongqing University, Chongqing 400044, China*
[2] *Chongqing University Three Gorges Hospital, Chongqing Municipality Clinical Research Center for Endocrinology and Metabolic Diseases, Chongqing 404000, China*
[3] *Institute of Life Sciences & Biomedical Collaborative Innovation Center of Zhejiang Province, Wenzhou University, Wenzhou 325035, China*
[4] *Department of Endocrinology, School of Medicine, Chongqing Emergency Medical Center, Chongqing University Central Hospital, Chongqing 400014, China*

Cite this article: *Nano Research*, **2025**, *18*, 94907078. https://doi.org/10.26599/NR.2025.94907078

ABSTRACT: Diabetes, a prevalent chronic metabolic disorder, often leads to severe complications. Currently, existing treatment methods may pose life-threatening risks due to poor patient compliance and inaccurate dosing of subcutaneous insulin injections. Hence, a biomimetic red blood cell (RBC) membrane-coated glucose-responsive nanoplatform is developed for controlling insulin release. Functionalizing nanoplatforms with RBC membrane can prolong the half-life of nano-formulation *in vivo* mediated by the biomimetic immune escape. Simultaneously, the cascade catalytic effect of glucose oxidase (GOx) encapsulated in metal-organic frameworks (MOFs) and hemoglobin (Hb) in the RBC membrane are able to not only facilitate glucose-responsive insulin release, but also eliminate the detrimental by-product hydrogen peroxide (H_2O_2) resulting from the Hb mediated H_2O_2 scavenging. Both *in vitro* and *in vivo* studies have demonstrated the favorable glucose-responsive performances of this advanced nano-platform with a single intravenous injection maintaining blood glucose balance in Type 1 Diabetes (T1D) mice for an extended duration without the hypoglycemia risk. Therefore, this biomimetic insulin delivery system is poised to function as a strategy for the intravenous insulin administration, offering a promising drug candidate for the self-adaptive long-term T1D treatment.

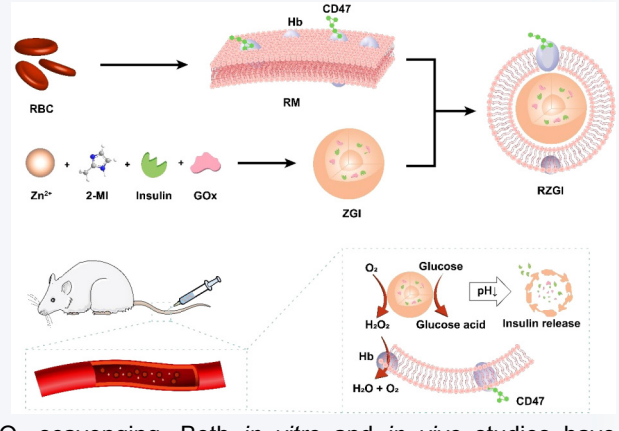

KEYWORDS: glucose-responsive, metal-organic frameworks, red blood cell membrane, insulin delivery, glucose oxidase, hemoglobin

1 Introduction

Diabetes is a prevalent metabolic disorder characterized by hyperglycemia resulting from insulin resistance or inadequate insulin secretion by the pancreas [1, 2]. It is often accompanied by a range of severe complications [3, 4]. Currently, the standard diabetes treatment relies on regular blood glucose level (BGL) monitoring and insulin injections. However, this continuous self-administration, known as an open-loop insulin delivery system, often results in poor compliance of patients and inadequate regulation of blood glucose [5, 6]. Recent advancements in insulin delivery systems, such as oral, transdermal, nasal, and pulmonary methods, have improved drug absorption, stability, and patient comfort [7–10]. However, these treatments continue to face challenges in precisely regulating BGLs and may still result in

Received: June 26, 2024; **Revised:** September 21, 2024
Accepted: October 17, 2024

✉Address correspondence to Wei Wu, david2015@cqu.edu.cn; Da Sun, sunday@wzu.edu.cn; Wuquan Deng, wuquandeng@cqu.edu.cn

serious side effects. Compared with a single insulin injection or continuous basal release, the ideal strategy is to increase insulin release during hyperglycemia and decrease it during hypoglycemia. Smart glucose-responsive insulin delivery systems, which integrate a glucose-sensing module with an insulin release module, represent a promising solution [11, 12]. In particular, chemically regulated smart glucose-responsive insulin delivery systems could facilitate insulin release in response to BGLs.

Glucose oxidase (GOx) is a flavin-containing glucose-specific enzyme capable of catalyzing glucose to produce hydrogen peroxide (H_2O_2) and gluconic acid in the presence of oxygen, leading to a gradual decrease in local pH [13, 14]. A decrease in local pH can accelerate the degradation of acid-sensitive carriers [15]. Therefore, co-loading insulin and glucose oxidase into a pH-sensitive carrier can facilitate insulin release under a hyperglycemia state [16]. Enzyme inactivation may occur during the preparation process, and the elevated production of H_2O_2 as a byproduct could potentially compromise enzyme activity and have damage risks to cell, tissue, or organs [17]. However, these are critical considerations in the development of glucose-responsive insulin delivery systems. Therefore, the selection of a pH-sensitive carrier that preserves enzyme activity while eliminating the side-effect product H_2O_2 is crucial for achieving sustained glucose-responsive insulin release.

Metal-organic frameworks (MOFs) are commonly utilized as nanocarriers for drug delivery and storage [18, 19]. These materials are crystalline porous structures that self-assemble from organic linkers and metal ions [20]. The rigid molecular structure and adjustable pore size of MOFs allow them to maintain strong biological activity even in severe environments and efficiently encapsulate proteins within their interior cavities [21, 22]. Furthermore, most MOFs can disassemble in response to specific stimuli such as acid, glutathione, adenosine triphosphate, etc., leading to sensitive drug release [17, 23–25].

Recently, biomimetic nanodrug carriers have been developed utilizing cell membrane-coated nanoparticles [17, 26]. These carriers offer advantages such as low immunogenicity, minimal side effects, and excellent biocompatibility, all while preserving the intricate surface structure and unique biological functions of cell membrane [27–29]. Red blood cell (RBC) possesses a long half-life in the circulation and excellent biocompatibility [30]. Consequently, nanoparticles enveloped with RBC membrane can significantly augment the retention of nanoparticles *in vivo* [31, 32]. CD47 is a transmembrane protein highly expressed on the surface of RBC, primarily serving as a self-protective mechanism to evade the immune system. Its ligand, the signaling regulatory protein α (SIRPα), is predominantly expressed in macrophages. When CD47 binds with SIRPα, it transmits a "do not eat me" inhibitory signal, effectively halting macrophages from engaging in phagocytic activity [33, 34]. Additionally, hemoglobin (Hb), the primary component of RBC, is essential for oxygen transport and energy metabolism. Specifically, Hb-containing peroxidase can catalyze the decomposition of H_2O_2, thus reducing oxidative damage [35]. Compared with other cell membranes, nanoparticle coated with RBC membrane is able to not only extend nanoparticle's retention time *in vivo* through CD47 but also scavenges H_2O_2 via Hb for further enhancing the therapeutic efficacy and safety.

Hence, in this study, a long-term and safe insulin controlled release system was constructed based on dynamic BGLs (Fig. 1). To establish a glucose-responsive insulin delivery system, GOx and insulin are co-loaded into zeolite imidazole framework-8 (ZIF-8), a widely used biodegradable MOF material known for its low toxicity and pH sensitivity. In this design, GOx catalyzes the conversion of glucose into gluconic acid and H_2O_2. The decrease of pH in the microenvironment triggers the degradation of ZIF-8, leading to the release of insulin. Subsequently, the functionalization of the RBC membrane coating not only accomplishes the biomimetic "endogenous" camouflage, but also decomposes the detrimental by-product H_2O_2 mediated by the Hb catalysis. Both *in vitro* and *in vivo* studies have demonstrated the favorable glucose-responsive properties of the nanoplatform, with a single intravenous injection maintaining blood glucose balance in Type 1 Diabetes (T1D) mice for an extended duration without the hypoglycemia risk. Therefore,

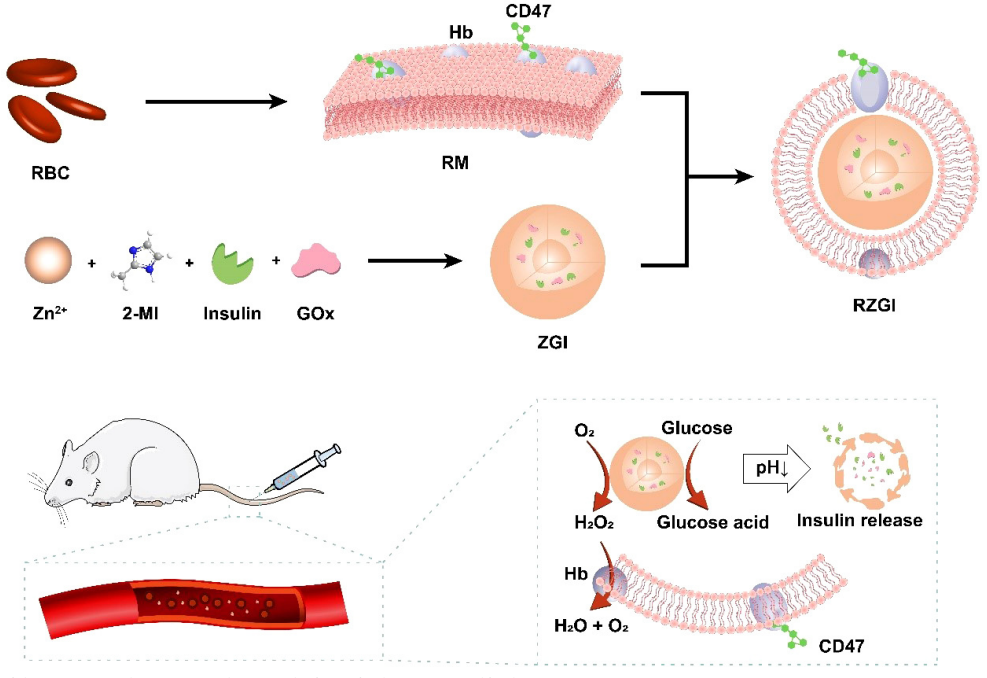

Figure 1 Illustration of the RBC membrane-coated nano-platform for long-term self-adaptive treatment in T1D.

this biomimetic nanoplatform is poised to function as a strategy for intravenous insulin administration, offering a promising drug candidate for the self-adaptive long-term T1D treatment.

2 Materials and methods

2.1 Chemical and materials

Zinc nitrate hexahydrate ($Zn(NO_3)_2{\cdot}6H_2O$) was obtained from Chron Chemicals (Chengdu, China). 2-Methylimidazole (2-MI) and insulin were obtained from Sigma (USA). Fluorescein isothiocyanate (FITC) was acquired from Aladdin (Shanghai, China). GOx and glucose were obtained from J&K Scientific (Beijing, China). The remaining chemicals and reagents were acquired from commercial suppliers and used as supplied.

2.2 Synthesis of ZGI

2 mL of 2-MI (1.4 M) containing 1 mg insulin was stirred. Then, 2 mL of $Zn(NO_3)_2{\cdot}6H_2O$ (20 mM) containing 1 mg GOx was added drop by drop and stirred for 1 h. Next, the product was washed three times by centrifugation (10,000 rpm, 5min). The product obtained after centrifugation was pure ZGI.

2.3 Preparation of the RBC membrane

Firstly, the whole blood from the mice was centrifuged (1000 rpm, 5 min), and after that suspended in 0.25× PBS for a half-hour at 4 ℃ to induce the RBC membrane rupture. Then, the mixture was centrifuged (10,000 rpm, 10 min) and collected the precipitate, and washed with phosphate buffer saline (PBS) until the solution without red color. After sonication for 10 min, the obtained membrane was extruded 10 times through 400 nm polycarbonate porous membrane. The RBC vesicles (RVs) were stored at 4 ℃.

2.4 Preparation of RZGI

RZGI was prepared by coating the RBC membrane on the surface of ZGI by extrusion. In brief, ZGI and RBC vesicles were mixed in specific ratios and sonicated for 5 min. Subsequently, the mixture was extruded through a 400 nm polycarbonate porous membrane ten times consecutively to prepare RZGI.

2.5 Characterizations of RZGI

The hydrated size and zeta potential of ZGI and RZGI were measured using Malvern Nano-ZS Zetasizer (Zetasizer Nano ZS 90, Malvern, UK). Transmission electron microscopy (TEM, Talos F200S Thermoscientific, Czech) was introduced to examine the morphology of nanoparticles. A fluorescence spectrophotometer was used to determine the entrapment efficiency (EE) and drug loading (DL) of RZGI (FL, RF-6000, Shimadzu, Japan).

Polyacrylamide gel electrophoresis (sodium dodecyl sulfate polyacrylamide gel electrophoresis (SDS-PAGE)) was used for characterizing membrane proteins. RBC membrane proteins were collected and separated using a Bio-Rad electrophoresis system. The samples were run for 25 min at 80 V and then for 60 min at 120 V. Ultimately, the polyacrylamide gel was visualized by overnight staining with SimplyBlue.

The presence of CD47 and Hb in the sample was assessed using western blot. The polyacrylamide gel, obtained through the initial preparation of SDS-PAGE, subsequently was electrically transferred onto a polyvinylidene fluoride (PVDF) membrane. The membrane will be initially incubated with primary antibodies and then incubated with horseradish peroxidase-labeled IgG. Protein signals were quantified through enhanced chemiluminescence and visualized using the ChemiDoc MP imaging system.

2.6 *In vitro* glucose-responsive drug release study

Firstly, insulin was modified with FITC to prepare insulin-FITC. FITC (5 mg/mL) was added dropwise to a gently stirred insulin solution (20 mg/mL) in 0.1 M calcium carbonate buffer, maintaining a molar ratio of 4:1 for FITC to insulin. The mixture was stirred for 3 h, followed by incubation without stirring for 0.5 h. The reaction mixture was dialyzed using a dialysis bag (MWCO: 1000 Da) against PBS for 6 h, and freeze-dried to obtain the pure insulin-FITC.

The drug release investigation from RZGI used the dialysis method. 1 mL of RZGI (FITC-modified insulin, 1 mg/mL) was added in a dialysis bag (MWCO: 14,000 Da). After that, the dialysis bag was immersed in solution containing glucose with the varying concentrations (0, 5, and 15 mM). At the predetermined intervals, 2 mL of the released solution was collected, and an equal volume of fresh release medium was added. Finally, the cumulative drug release profiles were calculated by measuring the fluorescence intensity according to the pre-established standard curve.

2.7 Biocompatibility assessment

Cytotoxicity and hemolysis assays were employed to assess the biocompatibility of ZGI and RZGI. For hemolysis evaluation, 100 μL of the diluted blood sample was incubated with the varying concentrations of ZGI and RZGI in PBS. After incubation at 37 ℃ for 1 h, the samples were centrifuged. The absorbance of the supernatant at 540 nm was measured using a microplate reader. For cytotoxicity evaluation, cell viability was calculated after co-incubation with varying concentrations of ZGI and RZGI at 37 ℃ for 24 h.

2.8 *In vitro* uptake by macrophages

RAW 264.7 cells were seeded into a 6-well plates. After 12 h, the RAW 264.7 cells were treated with ZGI-FITC or RZGI-FITC for 1 or 3 h (at 100 μg/mL insulin-FITC). Then, the culture medium was removed, and the cells were washed three times with PBS. The confocal laser scanning microscopy (CLSM) captured the fluorescent images. Fluorescence-activated cell sorting (FACS) was used to assess the quantitative fluorescence intensity of the cellular uptake.

2.9 H_2O_2 catalytic activity

The peroxidase activity of Hb was assessed by incubating various concentration of RVs, ZGI or RZGI with 2 mM ABTS and 0.1 mM H_2O_2. After 1 h, the absorbance at 418 nm was measured. Various concentrations of RVs, ZGI, or RZGI were incubated with 0.1 mM H_2O_2 for 1 h. Subsequently, ammonium molybdate was added. Finally, after further incubation for 10 min, the absorbance at 350 nm was measured to calculate the scavenging ratio of H_2O_2.

To assess the degradation of H_2O_2 by Hb *in vitro*, HUVECs were incubated with ZGI or RZGI for 1 h. Subsequently, 2,7-dichlorodihydrofluorescein diacetate (DCFH-DA) was added and incubated for 40 min and observed under a fluorescence microscopy. The fluorescence intensity was further quantified using FACS analysis.

2.10 *In vivo* study for T1D mice treatment

All of the mice feed and experimental agreement were carried out

with the approval of the Laboratory Animal Welfare and Ethics Committee of Chongqing University (IACUC Issue No.: CQU-IACUC-RE-202312-003). An animal model of T1D was induced by intraperitoneal injection of streptozotocin (STZ) [36, 37]. Briefly, male C57BL/6 mice were fasted for 18 h, and then intraperitoneally injected with 10 mg/mL of STZ solution (50 mg/kg). The BGLs of mice were monitored by a blood glucose meter (OneTouch Verio Flex). The model was considered to be successfully established when the BGLs higher than 11.1 mM for the consecutive three days. Each group consisted seven mice, and each mouse was treated with an intravenous injection of PBS, and the free insulin, ZGI, or RZGI with an equal insulin dosage of 2 mg/kg. Then, the BGLs were monitored at the predetermined intervals. The intraperitoneal glucose tolerance test (IPGTT) was used to assess the *in vivo* glucose responsiveness of RZGI. After overnight fasting, the T1D mice were intravenously injected with PBS, insulin, ZGI, or RZGI, while the healthy mice were treated with a PBS injection. After 1.5 h, the mice were intraperitoneally injected with a glucose solution (1.5 g/kg) and subsequently monitored the change tendency of blood glucose levels (BGLs).

2.11 Statistical analysis

The data were shown as mean ± SD. To assess potential differences among the groups, a one-way analysis of variance (ANOVA) followed by Tukey's test was performed. $^{*}p < 0.05$, $^{**}p < 0.01$, $^{***}p < 0.001$, and $^{****}p < 0.0001$ were used to indicate significance, or no significance (ns).

3 Results and discussion

3.1 Preparation and characterization of ZGI and RZGI

According to the reported literatures with a slight modification [17, 38], GOx and insulin were effectively encapsulated within ZIF-8 crystals using a one-pot method. Subsequently, the RBC membrane was coated on the surface of the ZGI through co-extrusion (Fig. 2(a)). From Fig. 2(b), the TEM images of ZGI and RZGI indicated the uniform spherical morphology. Interestingly, for RZGI, the cell membrane structures on the surface of nanoparticles were visually observed, suggesting the well-defined structure with the favorable cell membrane coating. Dynamic light scattering (DLS) was employed to measure the hydrated diameters of ZGI and RZGI. As shown in Fig. 2(c), the average diameters of ZGI and RZGI were approximately 162.0 and 249.3 nm, respectively. Meanwhile, the zeta potential of ZGI was –22.7 mV, while that of RZGI was –32.8 mV (Fig. 2(d)). Additionally, the confocal microscopy images showed that the Rho-modified GOx and FITC-modified insulin co-encapsulated ZIF-8 could well co-localize, further confirming that GOx and insulin were efficiently loaded into ZIF-8 (Fig. 2(e)). According to the fluorescence spectrophotometer measurement, the EE and DL of RZGI were 93.8% and 9.6%, respectively.

Given the inherent biological functions of RBC with the CD47 mediated immune escape, it was commonly accepted that the therapeutic nanomaterials coated with RBC membrane might attenuate the undesirable clearance by the immune system and prolong the blood retention time *in vivo* [31, 34]. SDS-PAGE analysis was employed to evaluate the protein retention of RBC membrane. As shown in Fig. 2(f), compared with the mother RBC membrane, RZGI demonstrated a nearly complete retention of all proteins. Moreover, the expression of key proteins including CD47 and Hb, was assessed by western blot analysis. The western blot result showed that CD47 and Hb were well retained on the surface of RZGI, suggesting that the RZGI had a great potential for retaining the biomimetic functions form RBC (Fig. 2(g)).

3.2 *In vitro* glucose-responsive drug release study

The release of insulin in response to glucose from RZGI depended on the disintegration of ZIF-8 triggered by the acidic micro-

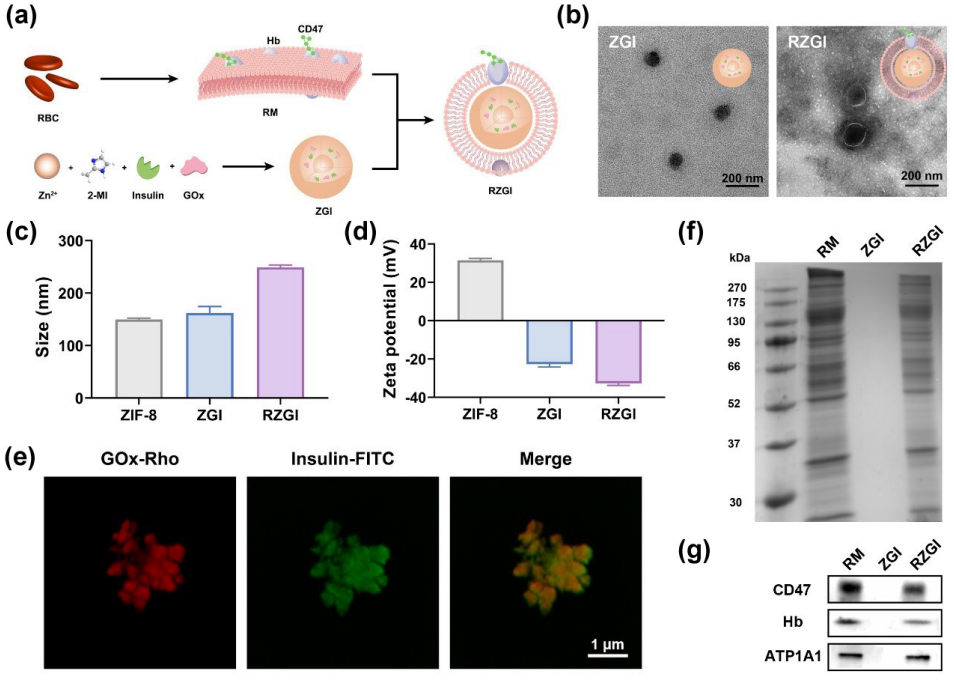

Figure 2 Synthesis and characterizations of nano-formulations. (a) The synthesis diagram of RZGI. (b) TEM images of ZGI and RZGI (scale bar was 200 nm). (c) The hydrated diameters and (d) zeta potential of ZIF-8, ZGI, and RZGI. (e) CLSM images of ZGI, GOx stained with Rhodamine B (red), and insulin marked with FITC (green) (scale bar was 1 μm). (f) SDS-PAGE of proteins for RM, ZGI, and RZGI. (g) Western blot analysis of CD47 and Hb in RM, ZGI, and RZGI.

environment (Fig. 3(a)), which was resulted from the GOx based catalyzing the conversion of glucose into gluconic acid [17, 38]. Hence, after RZGI mixed with glucose solution at varying concentrations, the pH value of the mixture was measured at different time intervals. As shown in Fig. 3(b), for RZGI immersed in a 15 mM glucose solution, the pH value dropped from 7.4 to 3.9 within 24 h. As the local pH eventually dropped, ZIF-8 was tended to degrade for promoting the loaded insulin release for the self-adaptive regulation of BGLs.

To assess the glucose-responsive release of insulin from RZGI, insulin was labeled with FITC. The dialysis method was employed to measure the release of insulin following the incubation of RZGI with glucose solutions with the varying concentrations. As shown in Fig. 3(c), the release content of insulin depended on both time and glucose concentration. In the high-concentration (15 mM) glucose solution, RZGI exhibited a fast insulin release with a cumulative release rate up to 71.1% within 12 h, which was extremely higher than that at low concentration (5 mM) of glucose, i.e., with a cumulative release rate to 41.4%. Even in the absence of glucose, insulin was slowly released (10.3% in 12 h), indicating a stable cargo encapsulation. Simultaneously, RZGI served as a "smart" and controllable nano-delivery system, i.e., the enhanced release of insulin at high glucose concentration while the slow release at low glucose concentrations, demonstrating the great promising for the self-adaptive glucose regulation (Fig. 3(d)). Furthermore, as the glucose specificity investigation, the enhanced insulin release from RZGI was specifically triggered by glucose, but not other sugars such as galactose, β-lactose, and sucrose (Fig. 3(e)). Meanwhile, the circular dichroism (CD) spectra result also demonstrated that the released insulin from RZGI well maintained the characteristic secondary structure of the native protein, suggesting the effective conformation and activity preservation of insulin (Fig. 3(f)).

3.3 *In vitro* biocompatibility assessment of RZGI

The biocompatibility of nanomedicine is a crucial property for biomedical applications. The MTS assay was used to evaluate the cytotoxicity of ZGI and RZGI. As shown in Fig. 4(a), after exposing HUVECs to both ZGI and RZGI with a high concentration up to 200 μg/mL, the cell viability was exceeded more than 80%, suggesting that neither ZGI nor RZGI exhibited the significant cytotoxic. For nanomedicines administered *in vivo*, the favorable hemolytic property is also crucial, as severe hemolysis could induce the life-threatening risks. The results of the hemolysis test indicated that both ZGI and RZGI with the high concentration up to 200 μg/mL showed the favorable low hemolysis less than 5% (Fig. 4(b) and Fig. S3 in the Electronic Supplementary Material (ESM)), confirming the superior biocompatibility of RZGI for potential applications *in vivo*.

3.4 *In vitro* uptake by macrophages

Macrophages possessed the capability to recognize and clear the foreign substances, including nanoparticles [33, 34]. Hence, the self-biomimetic ability of the RBC membrane-coated nanoparticles to evade recognition and clearance by macrophages was investigated. Therefore, ZGI and RZGI were labeled with FITC and incubated with macrophages. The fluorescence intensity of ZGI and RZGI internalized by macrophages was observed by CLSM. As shown in Fig. 4(c), the fluorescence intensity of the ZGI group was consistently higher than that of the RZGI group. Furthermore, the quantitative analysis using flow cytometry demonstrated that the fluorescence intensity of ZGI co-cultured with macrophages was 1.5 times higher than that of RZGI (Figs. 4(d)–4(f)), suggesting the effective immune escape of RZGI to prolong the blood circulation for facilitating the long-term glucose management *in vivo*.

3.5 H_2O_2 catalytic activity

GOx can catalyze glucose to produce the by-product H_2O_2, which leads to the oxidative stress for exacerbating the oxidative damage. Red blood cells with the abundant Hb as a peroxidase can degrade H_2O_2 into H_2O and O_2, reducing undesirable damage risks. Hence, the RBC membrane coated nanoparticles could not only act as the biomimetic "endogenous" camouflage, but also catalyze the decomposition of H_2O_2 mediated by Hb (Fig. 5(a)). As shown in Fig. 5(b), the evaluation results of peroxidase activity indicated that the absorbance of RZGI and RVs groups was increased with the

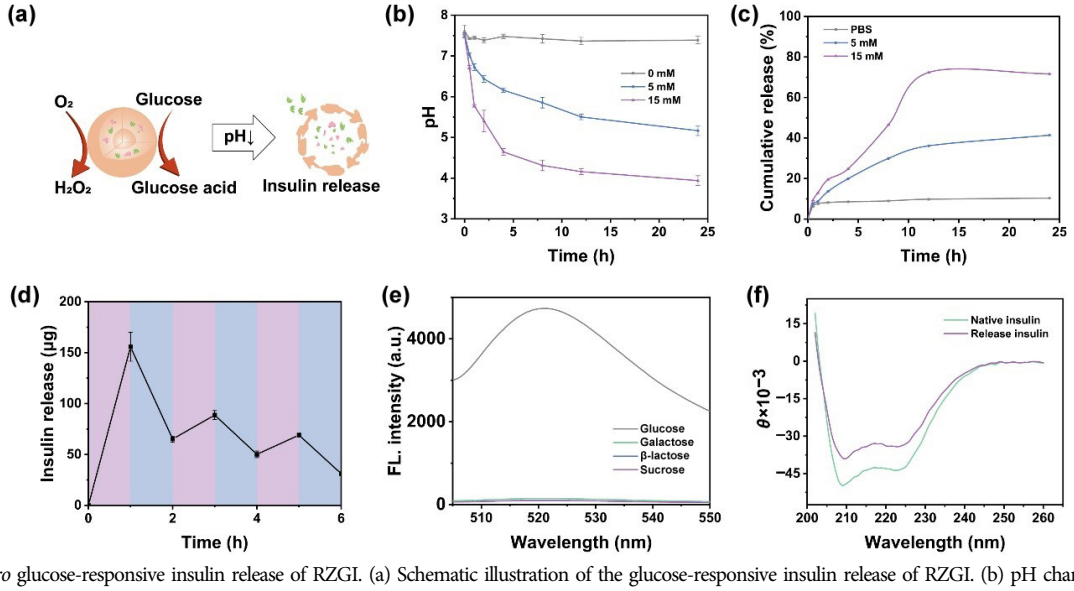

Figure 3 *In vitro* glucose-responsive insulin release of RZGI. (a) Schematic illustration of the glucose-responsive insulin release of RZGI. (b) pH changes tendency of RZGI immersed in the various concentrations of glucose. (c) Insulin release profiles of RZGI. (d) The release rate of insulin from RZGI with the self-adaptive glucose concentration. (e) Fluorescence spectra of RZGI incubated with glucose, galactose, β-lactose, and sucrose. (f) CD spectra of insulin before and after released from RZGI.

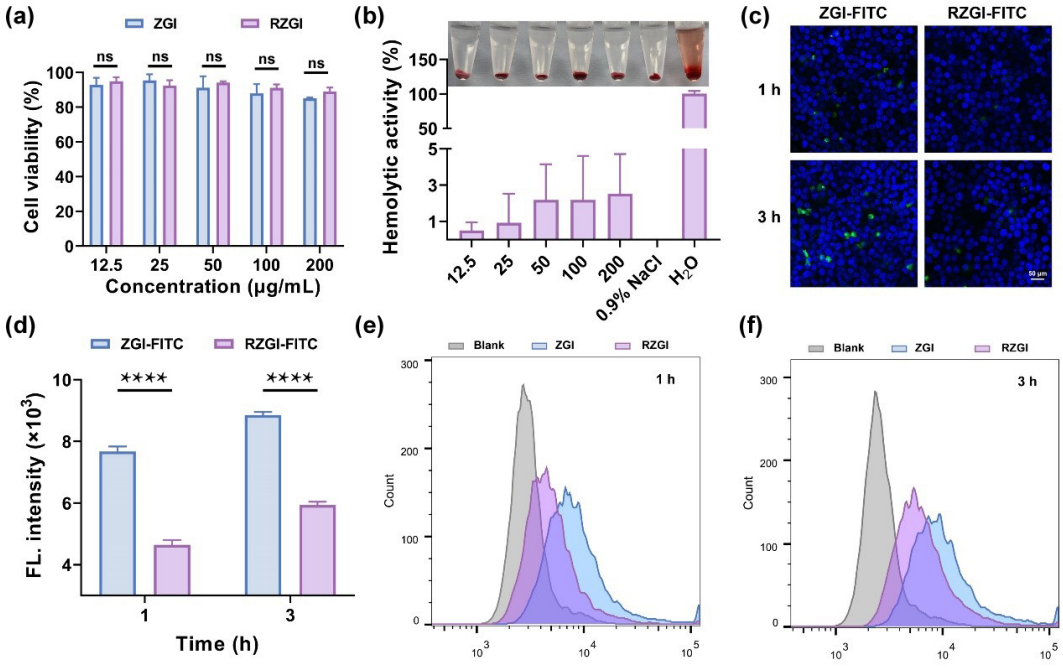

Figure 4 (a) Cell viability of HUVECs treatment with ZGI and RZGI, respectively, at 12.5, 25, 50, 100, and 200 μg/mL insulin (n = 3). (b) Visual observation diagram and statistical diagram of hemolysis results of RZGI at 12.5, 25, 50, 100, and 200 μg/mL insulin. (c) CLSM images of ZGI-FITC and RZGI-FITC incubated with RAW 264.7 cells, at 100 μg/mL insulin-FITC (scale bar was 50 μm). (d) Quantification of ZGI-FITC and RZGI-FITC incubated with RAW 264.7 cells (n = 3). FACS results of ZGI and RZGI uptake by RAW 264.7 cells at (e) 1 h or (f) 3 h. ns, no significance, and ****$p < 0.0001$.

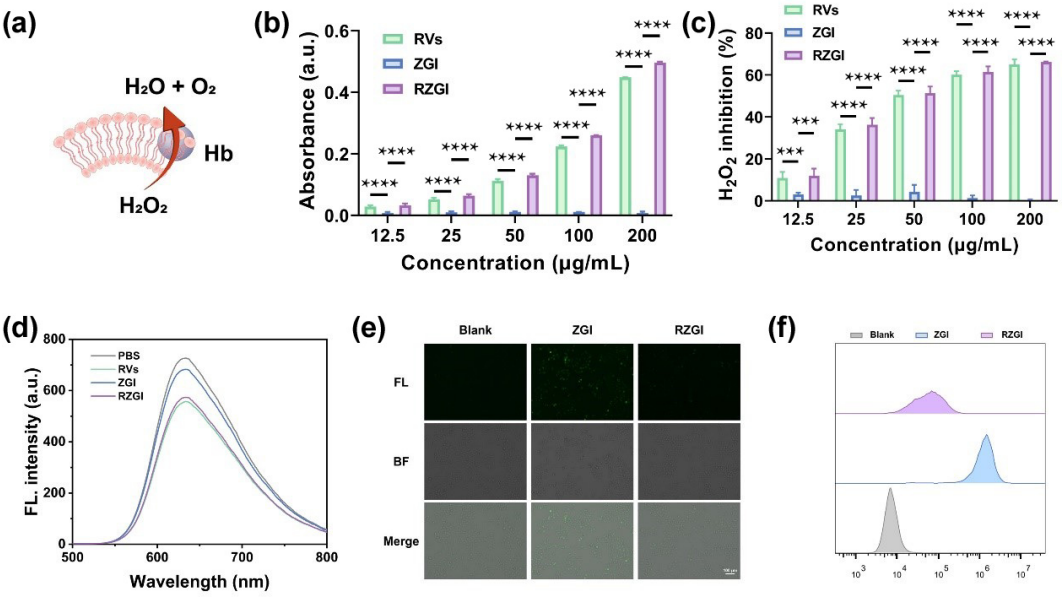

Figure 5 H_2O_2 catalytic activity of RZGI. (a) Schematic illustration of H_2O_2 scavenging by Hb. (b) RVs, ZGI, and RZGI-mediated peroxidation of ABTS (at 12.5, 25, 50, 100, and 200 μg/mL insulin). (c) The catalysis ability of RVs, ZGI, and RZGI for H_2O_2 (at 12.5, 25, 50, 100, and 200 μg/mL insulin). (d) Fluorescence spectra of $[Ru(dpp)_3]Cl_2$ after RVs, ZGI, and RZGI incubated with H_2O_2 (at 100 μg/mL insulin). (e) Fluorescence images of scavenging effects of H_2O_2 with ZGI and RZGI for 1 h, respectively, at 100 μg/mL insulin (scale bar was 100 μm). (f) FACS results of scavenging effects of H_2O_2 with ZGI and RZGI for 1 h, respectively, at 100 μg/mL insulin. ns, no significance, ***$p < 0.001$, and ****$p < 0.0001$.

increased concentration, indicating an elevated peroxidase activity. Besides, the ZGI group exhibited nearly no peroxidase activity across various concentration. As shown in Fig. 5(c), the scavenging activity of H_2O_2 by RZGI and RVs exhibited a concentration-dependent effect, whereas ZGI was demonstrated to be inactive to scavenge H_2O_2, indicating that Hb containing into the RBC membrane could effectively scavenge the undesirable by-product H_2O_2. Moreover, because the oxygen could quench the fluorescence of $[Ru(dpp)_3]Cl_2$, incubation of RVs and RZGI with H_2O_2 also could quench the fluorescence of $[Ru(dpp)_3]Cl_2$, further confirming that the Hb in RZGI could catalyze the H_2O_2 decomposition to produce oxygen (Fig. 5(d)). In addition, the H_2O_2 scavenging activity of RZGI was further assessed in HUVECs. As shown in Fig. 5(e), because the GOx catalysis produced H_2O_2 imaging using

DCFH-DA, a significant high green fluorescence was observed in cells incubated with ZGI, indicating an elevated level of H_2O_2 resulting from the glucose oxidation catalyzed by GOx. However, the fluorescence intensity of cells incubated with RZGI was significantly decreased, and the flow cytometry analysis also corroborated these findings (Fig. 5(f)), which further confirmed that the RBC membrane coating was able to effectively reduce the byproduct H_2O_2 and alleviate oxidative stress. Furthermore, as shown in Fig. S4 in the ESM, RZGI exhibited sustained H_2O_2 scavenging ability, which could significantly enhance the safety of the treatment.

3.6 *In vivo* study of RZGI for T1D mice treatment

For *in vivo* study, compared with insulin and ZGI consumed out in 4 and 8 h, respectively, RZGI could significantly prolong blood retention time, i.e., more than 9% of the relative fluoresce intensity could be detected after 24 h (Figs. 6(a) and 6(b)). The relative fluorescence signal intensity was calculated using the area under the curve. As shown in Fig. S5 in the ESM, RZGI exhibited significantly stronger fluorescence intensity compared with the insulin and ZGI over the first 8 h, which was attributed to the anti-phagocytic effect of CD47 retained on the RBC membrane. These results suggested that RZGI could prolong blood retention time and provide the sustained blood glucose regulation. Simultaneously, the *in vivo* distribution results revealed that the ZGI and RZGI were primarily distributed in the liver and kidney, with less accumulation observed in the heart, spleen, and lung (Fig. S6 in the ESM).

Subsequently, to assess the therapeutic efficacy of RZGI in T1D mice, STZ-induced T1D mice were intravenously administered insulin, ZGI, and RZGI. As shown in Figs. 6(c) and 6(d), the BGLs of mice treated with insulin decreased rapidly within the first 2 h, but rapidly returned to the high BGLs within 8 h, possibly attributing to the rapid diffusion of free insulin and the short half-life *in vivo*. The BGLs of mice injected with ZGI remained within the normal range for 8 h, followed by a gradual increase until reaching hyperglycemic levels after 24 h. For the mice treated with RZGI, the BGLs gradually decreased and remained within the normal range for 24 h, with some mice even maintaining normal BGLs until 2 day. As shown in Fig. S7 in the ESM, compared with intravenous injection, subcutaneous administration in TD1 mice demonstrated that ZGI and RZGI were less effective for regulating blood glucose, which might be ascribed to the limited content of nanoparticle delivering into the bloodstream, reducing their capacity to regulate blood glucose. These results demonstrated that RZGI was capable of improving the "smart" and sustained glucose-responsive insulin release for efficiently self-adaptive management of BGLs *in vivo*.

Moreover, IPGTT was employed to assess the dynamics of insulin release *in vivo*. As shown in Fig. 6(e), the BGLs of mice returned to normal at 1.5 h after treatment with insulin, ZGI, and RZGI. Subsequently, following an intraperitoneal injection of a glucose solution (1.5 g/kg), the BGLs of mice were further monitored. After the injection of a glucose solution in healthy mice, the BGLs gradually increased to 8.4 mM after 0.5 h and rapidly returned to normal levels within 1.5 h. However, the BGLs of T1D mice treated with insulin rapidly rose to 13.6 mM within 0.5 h and remained in a hyperglycemic state. Notably, the BGLs of T1D mice treated with ZGI and RZGI increased to 11.1 and 10.5 mM, respectively, within 0.5 h, and then gradually decreased to a normoglycemia state. Afterward, the glucose response of mice to the various treatments was assessed by calculating the area under the BGLs curves for each group. As shown in Fig. 6(f), compared with insulin treatment, both ZGI and RZGI improved the responsiveness of IPGTT, exhibiting a similar responsiveness to that of healthy mice. In addition, the long-term IPGTT results showed that both ZGI and RZGI improved responsiveness compared with insulin treatment (Fig. S8 in the ESM). The superior effect of RZGI could be attributed to the RBC membrane coating, which prolonged blood retention time *in vivo*.

Investigating the potential toxicity of nanomedicines *in vivo* is crucial, including the assessment of parameters such as body weight, blood routine, and histopathological evaluation. The weight of mice did not exhibit significant changes in this experimental investigation, indicating that ZGI and RZGI did not induce any apparent side effects on the weight of mice (Fig. S9 in the ESM). To further validate safety *in vivo*, organ sections from mice were isolated, stained with hematoxylin and eosin (H&E), and examined

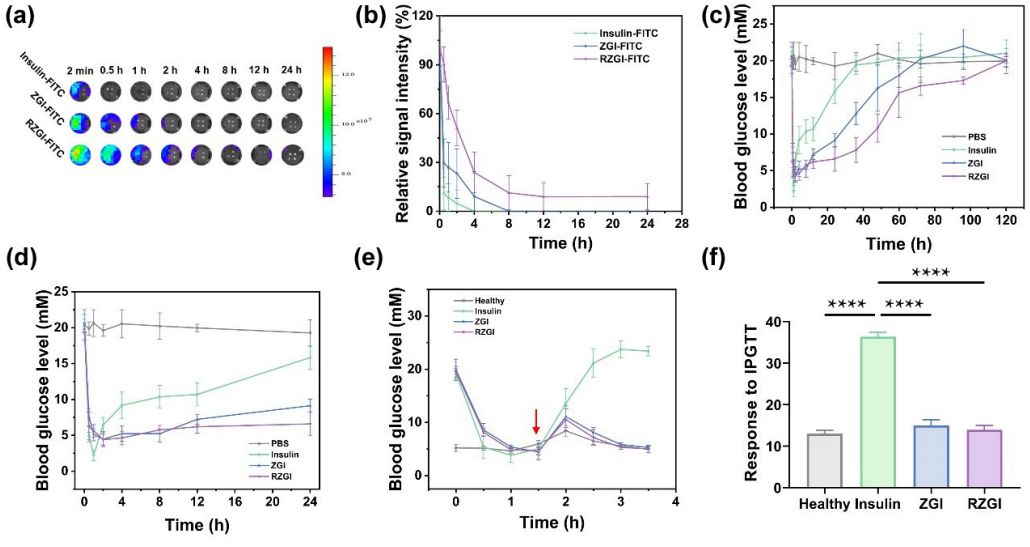

Figure 6 *In vivo* study of formulations for T1D mice treatment. (a) Fluorescence images and (b) quantification analysis of insulin-FITC, ZGI-FITC, and RZGI-FITC. (c) and (d) BGLs of T1D mice after treatment with PBS, free insulin, ZGI, and RZGI. (e) The IPGTT test of free insulin, ZGI and RZGI in healthy mice and T1D mice. The red arrow indicates the time of IPGTT injection. (f) The IPGTT responsiveness was calculated for the area under the curve between 1.5 and 3.5 h. ***$p < 0.001$.

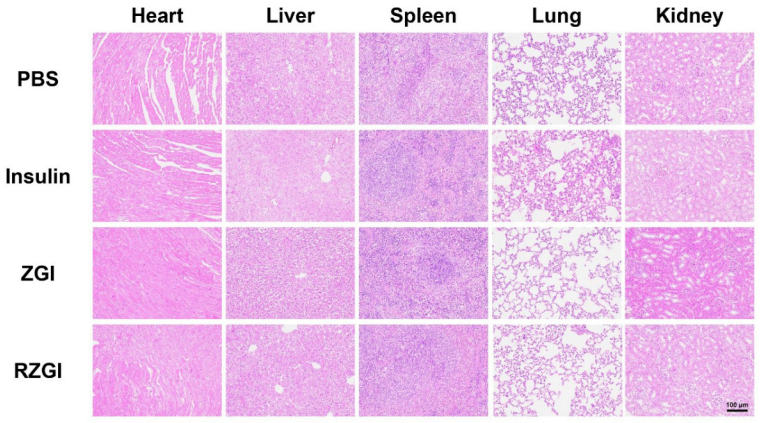

Figure 7 H&E staining of the main organs in mice (scale bar was 100 μm).

for histological morphology. As shown in Fig. 7, the treatment groups did not show any apparent pathological signs in terms of tissue morphology, inflammation, and structure. In addition, there was no significant differences in blood routine between the treatment groups and the PBS group (Fig. S10 in the ESM). The above mentioned analyses further demonstrated that ZGI and RZGI exhibited good biocompatibility without any apparent side effects.

4 Conclusions

In summary, we have constructed a biomimetic insulin delivery system comprising the GOx and insulin co-loaded ZIF-8 with the surficial RBC membrane coating, enabling glucose-responsive insulin release for the self-adaptive BGLs management. The RBC membrane coating not only provided "endogenous" biomimetic functions for prolonging blood circulation time, but also catalyzed the decomposition of the undesirable by-product H_2O_2 mediated by Hb from the RBC membrane. The resulting biomimetic insulin delivery system, RZGI, exhibited a favorable performance, such as the well-defined nano-formulation with uniform size, negative charge, glucose-responsive insulin release, H_2O_2 catalytic activity, and immune escape *in vitro*. Besides, *in vivo* studies also confirmed that RZGI with a single intravenous injection could sustain blood glucose balance in T1D mice for an extended duration without the risk of hypoglycemia. Hence, this biomimetic insulin delivery system is a great promising candidate as an intravenous insulin nano-formulation for self-adaptive long-term T1D management.

Electronic Supplementary Material: Supplementary material (TEM images of ZIF-8; standard curve of the fluorescence intensity in different concentrations of insulin-FITC; hemolysis results of ZGI; additional FACS results; relative fluorescence intensity of insulin-FITC, ZGI-FITC, and RZGI-FITC in blood after injection; fluorescence signal accumulated in main organs after injection insulin-FITC, ZGI-FITC, and RZGI-FITC; subcutaneous administration results; fluorescence intensity of long-term IPGTT; weight changes of mice during treatment; blood routine of mice with different treatments) is available in the online version of this article at https://doi.org/10.26599/NR.2025.94907078.

Data availability

All data needed to support the conclusions in the paper are presented in the manuscript and the Electronic Supplementary Material. Additional data related to this paper may be requested from the corresponding author upon request.

Acknowledgements

Funds from the National Natural Science Foundation of China (Nos. 32171324 and 31971301) helped to support this work, Fundamental Research Funds for Central Universities (Nos. 2024CDJXY017 and 2023CDJXY-051), Fundamental Research Funds for the National Key R&D Project (No. 2022YFF0710700), 2030 Major Research Projects for Technological Innovation (No. 2023ZD0509402), and Natural Science Foundation of Chongqing (Nos. 2022NSCQ-BHX4850, CSTB2022NSCQ-BHX0718, and CSTB2022NSCQ-BHX0724).

Declaration of competing interest

The authors declare no conflict of interest.

Author contribution statement

S. W.: Methodology, formal analysis, investigation, writing original draft. L. Z.: Conceptualization, writing-review and editing, supervision. S. N.: Methodology, investigation, validation. X. Z.: Methodology, investigation, data curation. M. Y.: Methodology, investigation. Y. Z.: Methodology, investigation, validation. K. K.: Investigation, data curation. Y. L.: Investigation, resources. K. W. B.: Methodology, investigation. K. Q.: Methodology, investigation, data curation. X. Q.: Methodology, investigation, resources. K. Z.: Methodology, investigation, data curation. W. Q. D.: Conceptualization, writing – review & editing, supervision, funding acquisition. D. S.: Conceptualization, writing – review & editing, supervision, funding acquisition. W. W.: Conceptualization, writing – review & editing, supervision, project administration, funding acquisition. All the authors have approved the final manuscript.

Informed consent

Not applicable.

Ethics statement

All of the animals feed and experimental agreement were carried out with the approval of the Laboratory Animal Welfare and Ethics Committee of Chongqing University (IACUC Issue No.: CQU-IACUC-RE-202312-003).

Use of AI statement

None.

References

[1] Wang, Y. N.; Wang, C. H.; Li, K. Y.; Song, X. Y.; Yan, X. F.; Yu, L. M.; He, Z. Y. Recent advances of nanomedicine-based strategies in diabetes and complications management: Diagnostics, monitoring, and therapeutics. *J. Controlled Release* **2021**, *330*, 618–640.

[2] Wang, C.; Ye, Y. Q.; Sun, W. J.; Yu, J. C.; Wang, J. Q.; Lawrence, D. S.; Buse, J. B.; Gu, Z. Red blood cells for glucose-responsive insulin delivery. *Adv. Mater.* **2017**, *29*, 1606617.

[3] Ahlqvist, E.; Van Zuydam, N. R.; Groop, L. C.; McCarthy, M. I. The genetics of diabetic complications. *Nat. Rev. Nephrol.* **2015**, *11*, 277–287.

[4] Wu, S.; Zhu, L.; Ni, S.; Zhong, Y.; Qu, K.; Qin, X.; Zhang, K.; Wang, G. X.; Sun, D.; Deng, W. Q. et al. Hyaluronic acid-decorated curcumin-based coordination nanomedicine for enhancing the infected diabetic wound healing. *Int. J. Biol. Macromol.* **2024**, *263*, 130249.

[5] Zhang, Y. Q.; Yu, J. C.; Kahkoska, A. R.; Wang, J. Q.; Buse, J. B.; Gu, Z. Advances in transdermal insulin delivery. *Adv. Drug Deliv. Rev.* **2019**, *139*, 51–70.

[6] Ren, C. J.; Zhong, D. N.; Qi, Y. C.; Liu, C. Y.; Liu, X. Y.; Chen, S. H.; Yan, S.; Zhou, M. Bioinspired pH-responsive microalgal hydrogels for oral insulin delivery with both hypoglycemic and insulin sensitizing effects. *ACS Nano* **2023**, *17*, 14161–14175.

[7] Yu, J. C.; Zhang, Y. Q.; Ye, Y. Q.; DiSanto, R.; Sun, W. J.; Ranson, D.; Ligler, F. S.; Buse, J. B.; Gu, Z. Microneedle-array patches loaded with hypoxia-sensitive vesicles provide fast glucose-responsive insulin delivery. *Proc. Nat. Acad. Sci. USA* **2015**, *112*, 8260–8265.

[8] Sarmento, B.; Ribeiro, A.; Veiga, F.; Sampaio, P.; Neufeld, R.; Ferreira, D. Alginate/chitosan nanoparticles are effective for oral insulin delivery. *Pharm. Res.* **2007**, *24*, 2198–2206.

[9] Andrade, F.; das Neves, J.; Gener, P.; Schwartz, S. Jr. ; Ferreira, D.; Oliva, M.; Sarmento, B. Biological assessment of self-assembled polymeric micelles for pulmonary administration of insulin. *Nanomed: Nanotechnol., Biol. Med.* **2015**, *11*, 1621–1631.

[10] Martins, J. P.; Figueiredo, P.; Wang, S. Q.; Espo, E.; Celi, E.; Martins, B.; Kemell, M.; Moslova, K.; Mäkilä, E.; Salonen, J. et al. Neonatal Fc receptor-targeted lignin-encapsulated porous silicon nanoparticles for enhanced cellular interactions and insulin permeation across the intestinal epithelium. *Bioact. Mater.* **2022**, *9*, 299–315.

[11] Wang, S. Q.; Yang, C. W.; Zhang, W. T.; Zhao, S.; You, J. H.; Cai, R. S.; Wang, H.; Bao, Y. H.; Zhang, Y.; Zhang, J. et al. Glucose-responsive microneedle patch with high insulin loading capacity for prolonged glycemic control in mice and minipigs. *Acs Nano* **2024**, *18*, 26056–26065.

[12] Ji, K. F.; Wei, X. Q.; Kahkoska, A. R.; Zhang, J.; Zhang, Y.; Xu, J. C.; Wei, X. W.; Liu, W.; Wang, Y. F.; Yao, Y. J. et al. An orally administered glucose-responsive polymeric complex for high-efficiency and safe delivery of insulin in mice and pigs. *Nat. Nanotechnol*., in press, https://doi.org/10.1038/s41565-024-01764-5.

[13] Bakh, N. A.; Cortinas, A. B.; Weiss, M. A.; Langer, R. S.; Anderson, D. G.; Gu, Z.; Dutta, S.; Strano, M. S. Glucose-responsive insulin by molecular and physical design. *Nat. Chem.* **2017**, *9*, 937–944.

[14] Wang, J. Q.; Ye, Y. Q.; Yu, J. C.; Kahkoska, A. R.; Zhang, X. D.; Wang, C.; Sun, W. J.; Corder, R. D.; Chen, Z. W.; Khan, S. A. et al. Core–shell microneedle gel for self-regulated insulin delivery. *ACS Nano* **2018**, *12*, 2466–2473.

[15] Chen, G. S.; Huang, S. M.; Kou, X. X.; Wei, S. B.; Huang, S. Y.; Jiang, S. Q.; Shen, J.; Zhu, F.; Ouyang, G. F. A convenient and versatile amino-acid-boosted biomimetic strategy for the nondestructive encapsulation of biomacromolecules within metal-organic frameworks. *Angew. Chem., Int. Ed.* **2019**, *58*, 1463–1467.

[16] Zhang, Y. Q.; Wang, J. Q.; Yu, J. C.; Wen, D.; Kahkoska, A. R.; Lu, Y.; Zhang, X. D.; Buse, J. B.; Gu, Z. Bioresponsive microneedles with a sheath structure for H_2O_2 and pH cascade-triggered insulin delivery. *Small* **2018**, *14*, 1704181.

[17] He, M. Y.; Yu, P.; Hu, Y. L.; Zhang, J.; He, M. M.; Nie, C. P.; Chu, X. Erythrocyte-membrane-enveloped biomineralized metal-organic framework nanoparticles enable intravenous glucose-responsive insulin delivery. *ACS Appl. Mater. Interfaces* **2021**, *13*, 19648–19659.

[18] Mallakpour, S.; Nikkhoo, E.; Hussain, C. M. Application of MOF materials as drug delivery systems for cancer therapy and dermal treatment. *Coord. Chem. Rev.* **2022**, *451*, 214262.

[19] Lawson, H. D.; Walton, S. P.; Chan, C. Metal-organic frameworks for drug delivery: A design perspective. *ACS Appl. Mater. Interfaces* **2021**, *13*, 7004–7020.

[20] Furukawa, H.; Cordova, K. E.; O'Keeffe, M.; Yaghi, O. M. The chemistry and applications of metal-organic frameworks. *Science* **2013**, *341*, 1230444.

[21] Peng, S.; Bie, B. L.; Sun, Y. Z. S.; Liu, M.; Cong, H. J.; Zhou, W. T.; Xia, Y. C.; Tang, H.; Deng, H. X.; Zhou, X. Metal-organic frameworks for precise inclusion of single-stranded DNA and transfection in immune cells. *Nat. Commun.* **2018**, *9*, 1293.

[22] Feng, D. W.; Liu, T. F.; Su, J.; Bosch, M.; Wei, Z. W.; Wan, W.; Yuan, D. Q.; Chen, Y. P.; Wang, X.; Wang, K. C. et al. Stable metal-organic frameworks containing single-molecule traps for enzyme encapsulation. *Nat. Commun.* **2015**, *6*, 5979.

[23] Wang, R. F.; Qiu, M. S.; Zhang, L.; Sui, M.; Xiao, L.; Yu, Q.; Ye, C. H.; Chen, S. Z.; Zhou, X. Augmenting immunotherapy via bioinspired MOF-based ROS homeostasis disruptor with nanozyme‐cascade reaction. *Adv. Mater.* **2023**, *35*, 2306748.

[24] Yu, C. X.; Zhu, W. Y.; He, Z. Z.; Xu, J.; Fang, F. Y.; Gao, Z. A.; Ding, W. L.; Wang, Y. X.; Wang, J.; Wang, J. Q. et al. ATP-triggered drug release system based on ZIF-90 loaded porous poly (lactic-co-glycolic acid) microspheres. *Colloids Surf. A: Physicochem Eng Aspects* **2021**, *615*, 126255.

[25] Cheng, R. Y.; Jiang, L. X.; Gao, H.; Liu, Z. H.; Mäkilä, E.; Wang, S. Q.; Saiding, Q.; Xiang, L.; Tang, X. M.; Shi, M. M. et al. A pH-responsive cluster metal-organic framework nanoparticle for enhanced tumor accumulation and antitumor effect. *Adv. Mater.* **2022**, *34*, 2203915.

[26] Wang, Y.; Zhang, K.; Qin, X.; Li, T. H.; Qiu, J.; Yin, T. Y.; Huang, J. L.; McGinty, S.; Pontrelli, G.; Ren, J. et al. Biomimetic nanotherapies: Red blood cell based core–shell structured nanocomplexes for atherosclerosis management. *Adv. Sci. (Weinh)* **2019**, *6*, 1900172.

[27] Zhang, Q. Z.; Dehaini, D.; Zhang, Y.; Zhou, J. L.; Chen, X. Y.; Zhang, L. F.; Fang, R. H.; Gao, W. W.; Zhang, L. F. Neutrophil membrane-coated nanoparticles inhibit synovial inflammation and alleviate joint damage in inflammatory arthritis. *Nat. Nanotech.* **2018**, *13*, 1182–1190.

[28] Han, H. J.; Bártolo, R.; Li, J. C.; Shahbazi, M. A.; Santos, H. A. Biomimetic platelet membrane-coated nanoparticles for targeted therapy. *Eur. J. Pharm. Biopharm.* **2022**, *172*, 1–15.

[29] Fontana, F.; Molinaro, G.; Moroni, S.; Pallozzi, G.; Ferreira, M. P. A.; Tello, R. P.; Elbadri, K.; Torrieri, G.; Correia, A.; Kemell, M. et al. Biomimetic platelet-cloaked nanoparticles for the delivery of anti-inflammatory curcumin in the treatment of atherosclerosis. *Adv. Healthcare Mater.* **2024**, *13*, 2302074.

[30] Tan, S. W.; Wu, T. T.; Zhang, D.; Zhang, Z. P. Cell or cell membrane-based drug delivery systems. *Theranostics* **2015**, *5*, 863–881.

[31] Sun, X. Q.; Wang, C.; Gao, M.; Hu, A. Y.; Liu, Z. Remotely controlled red blood cell carriers for cancer targeting and near-infrared

light-triggered drug release in combined photothermal-chemotherapy. *Adv. Funct. Mater.* **2015**, *25*, 2386–2394.

[32] Castro, F.; Martins, C.; Silveira, M. J.; Moura, R. P.; Pereira, C. L.; Sarmento, B. Advances on erythrocyte-mimicking nanovehicles to overcome barriers in biological microenvironments. *Adv. Drug Delivery Rev.* **2021**, *170*, 312–339.

[33] Rodriguez, P. L.; Harada, T.; Christian, D. A.; Pantano, D. A.; Tsai, R. K.; Discher, D. E. Minimal "Self" peptides that inhibit phagocytic clearance and enhance delivery of nanoparticles. *Science* **2013**, *339*, 971–975.

[34] Sun, D.; Chen, J.; Wang, Y.; Ji, H.; Peng, R. Y.; Jin, L. B.; Wu, W. Advances in refunctionalization of erythrocyte-based nanomedicine for enhancing cancer-targeted drug delivery. *Theranostics* **2019**, *9*, 6885–6900.

[35] Liu, S. Y.; Zhang, Y. W.; Li, M.; Xiong, L.; Zhang, Z. J.; Yang, X. H.; He, X. X.; Wang, K. M.; Liu, J. B.; Mann, S. Enzyme-mediated nitric oxide production in vasoactive erythrocyte membrane-enclosed coacervate protocells. *Nat. Chem.* **2020**, *12*, 1165–1173.

[36] Wang, T.; Li, Y. R.; Cornel, E. J.; Li, C.; Du, J. Z. Combined antioxidant-antibiotic treatment for effectively healing infected diabetic wounds based on polymer vesicles. *ACS Nano* **2021**, *15*, 9027–9038.

[37] Zhao, H.; Huang, J.; Li, Y.; Lv, X. J.; Zhou, H. T.; Wang, H. R.; Xu, Y. Y.; Wang, C.; Wang, J.; Liu, Z. ROS-scavenging hydrogel to promote healing of bacteria infected diabetic wounds. *Biomaterials* **2020**, *258*, 120286.

[38] Zhang, C.; Hong, S.; Liu, M. D.; Yu, W. Y.; Zhang, M. K.; Zhang, L.; Zeng, X.; Zhang, X. Z. pH-sensitive MOF integrated with glucose oxidase for glucose-responsive insulin delivery. *J. Controlled Release* **2020**, *320*, 159–167.